ISBN: 978-3-95450-184-7 doi:10.18429/JACoW-IPAC2018-WEXGBF3

RF SYSTEM FOR FRIB ACCELERATOR*

D. Morris†, J. Brandon, M. Konrad, T. Larter, H. Maniar, E. Pozdeyev, H. Ren, S. Zhao,
Facility for Rare Isotope Beams, Michigan State University, East Lansing 48824, USA
N. Bultman, K. Davidson, P. Gibson, L. Hodges, P. Morrison, P. Ostroumov, J. Popielarski, T. Russo, K. Schrock, R. Walker, J. Wei, T. Xu, Y. Xu,
Facility for Rare Isotope Beams, Michigan State University, East Lansing 48824, USA
A. Facco, Laboratori Nazionali di Legnaro, Legnaro (Padova), Italy

Abstract

The RF system of the FRIB driver accelerator includes solid state amplifiers up to 18 kW operating at frequencies from 80.5 MHz to 322 MHz. Much higher power is required for the normal conducting RFQ, ~100 kW, and it is based on vacuum tubes. This invited talk presents the performance of solid state amplifiers and LLRF in off-line testing and on-line testing of the RFQ amplifier.

INTRODUCTION

The Facility for Rare Isotope Beams at Michigan State University will be a scientific user facility for nuclear physics research [1]. The FRIB linac consists of a room-temperature front end and a superconducting RF linac that will accelerate stable ion beams (from protons to uranium) to energies >200 MeV/u and at continuous wave beam power up to 400 kW. Figure 1 shows the layout of FRIB linac.

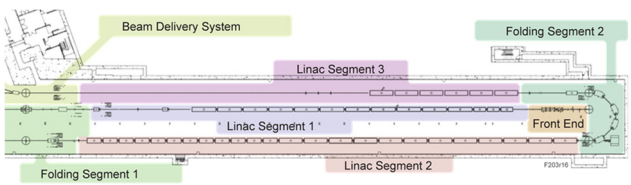

Figure 1: FRIB linac layout.

The ARTEMIS room temperature electron cyclotron resonance (ECR) ion source in the front end utilizes an 18 GHz Klystron transmitter. The Low Energy Beam Transport (LEBT) multi-harmonic buncher (MHB) operates at the three harmonics: 40.25, 80.5, and 120.75 MHz. Next, the Radio Frequency Quadrupole (RFQ) and two room temperature Medium Energy Beam Transport (MEBT) bunchers operate at 80.5 MHz. The front end was commissioned and is operating at or above KPP levels [2].

The super conducting RF linac includes four types of SRF cavities consisting of 104 quarter-wave resonators (QWR) and 220 half-wave resonators (HWR), operating at 80.5 MHz and 322 MHz, respectively. The first folding segment has two multi-gap operating at 161 MHz. Except for the Klystron and RFQ final stage amplifier, which uses a Thales TH-781 tetrode, the RF amplifiers are solid-state. Table 1 is a summary of the FRIB linac RF systems.

* This work is supported by the U.S. Department of Energy Office of Science under Cooperative Agreement DE-SC0000661 #wei@frib.msu.edu
† morrisd@frib.msu.edu.

Table 1: FRIB linac RF systems

System	Area	Frequency	Type	Required RF Power	Tuner	Qty
LEBT Multi-Harmonic Buncher (f1, f2, f3)	FE	40.25 MHz - 120.75 MHz	RT	100W	N/A	3
RFQ Driver	FE	80.5 MHz	RT	8 kW	N/A	1
RFQ Final (Tetrode)	FE	80.5 MHz	RT	100 kW	Servo (water)	1
MEBT Buncher	FE	80.5 MHz	RT	4 kW	2-phase stepper	2
β=0.041 (accelerating)	LS1	80.5 MHz	SC	700 W	2-phase stepper	12
β=0.085 (accelerating and matching)	LS1 - FS1	80.5 MHz	SC	2.5 kW	2-phase stepper	92
IH Multi-Gap Buncher	FS1	161 MHz	RT	18 kW	5-phase stepper	2
β=0.285 (accelerating and matching)	LS2	322 MHz	SC	3.0 kW	Pneumatic	72
β=0.530 (accelerating and matching)	LS2- LS3	322 MHz	SC	5.0 kW	Pneumatic	148

RF SYSTEM DESCRIPTION

The main components of the RF system are the reference clock distribution system, low level RF controllers, RF amplifiers, and high power transmission lines. Optional components include tuners (stepper motor, pneumatic valve, servo), spark detectors, and high voltage bias tees. Figure 2 shows the RF block diagram for a beta=0.085 SRF cavity.

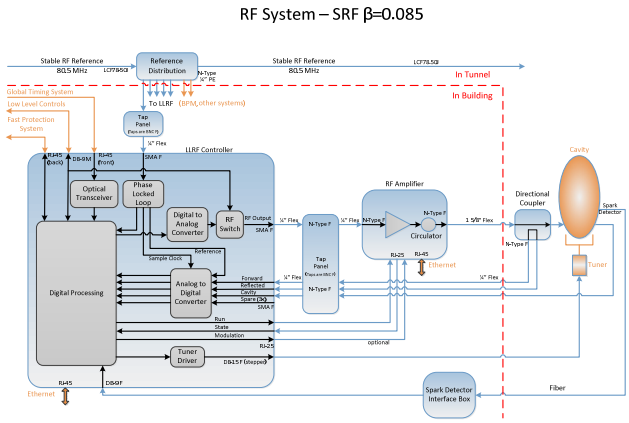

Figure 2: RF block diagram for SRF cavity.

LLRF Controllers

The FRIB LLRF controllers are used for cavity testing, integrated tests and cryomodule tests. In the past few years, different issues were found in both RF and tuner control. Many improvements have been made to resolve those issues, including smooth transition from open to close loop for RF control [3], valve open/close voltage calibration for pneumatic tuner control, stepper motor current settings, etc. Figure 3 shows the FRIB LLRF controller.

ISBN: 978-3-95450-184-7 doi:10.18429/JACoW-IPAC2018-WEXGBF3

Figure 3: FRIB LLRF controller. 1. Power supply; 2. Tuner board; 3. RF board; 4. FRIB general purpose digital board (FGPDB); 5. Front panel and board.

The FRIB LLRF controller supports both self-excited loop (SEL) mode and generator driven mode. The working range of SEL mode is +/− 50 kHz. The SEL mode helps to bring up the field even when the cavity is detuned from the reference frequency, and is used during the cavity turn on sequence (see Table 2).

Table 2: QWR Turn On Sequence

	RF	Amplitude	Amplitude Set-point	Phase	Tuner
Stage 1	**ON**	Open	Initial	SEL	OFF
Stage 2	ON	Open	Initial	SEL	**ON**
Stage 3	ON	Open	Initial	**Open**	ON
Stage 4	ON	**Close**	Initial	Open	ON
Stage 5	ON	Close	Initial	**Close**	ON
Stage 6	ON	Close	**Final**	Close	ON

For amplitude and phase regulation, the controller adopts the active disturbance rejection control (ADRC) algorithm [4]. Two types of tuner boards with the same form factor were designed for different type of cavities. The stepper tuner board is used for the quarter wave resonators. The analog tuner board is used for pneumatic valves (for HWRs) and servos (error signal to RFQ water skid).

The FRIB LLRF controller interfaces with multiple systems, including global timing system (GTS), fast protection system (FPS), low level control (LLC) system, experimental physics and industrial control system (EPICS) and the RF amplifier. The LLRF output will be interlocked based on the states of the above interfaces. For example, FPS not permitted, LLC not OK (vacuum/temperature bad), and amplifier fault. The LLRF also detects fault conditions based on its internal information. Internally generated interlocks include: fast drop of cavity field (usually caused by spark), cavity field low (due to multipacting), excessive cavity field (protects cavity from quenching), excessive forward power, excessive reflected power (protects amplifier), etc.

As mentioned earlier, multiple issues were found during various tests. An internal variable overflow in the FPGA implementation of the amplitude control loop [5] was found to be causing amplitude instability during power ramp-up. It was solved by an improved implementation of the control algorithm. The stepper board driver IC overheating was another problem found during the QWR prototype croymodule test. The stepper driver stopped working due to high current setting and insufficient cooling. The stepper tuner board was redesigned with better thermal management (heat sinks on both sides of the driver IC). The current setting was also adjusted according to the stepper motor specification.

During the integrated test for the β=0.53 HWR, the cavity frequency control with the pneumatic tuner was not good due to the lack of experience with the nonlinear behaviour of the valve characteristic. After consulting with experts at the Argonne National Laboratory (ANL), a procedure has been developed to calibrate the valve open/close voltages for the pneumatic tuner. First, the set screws are adjusted to fully close (or open) the values when applying 0% (or 100%) control voltage. Next, the close voltages for both valves are set to the zero offset point (see Figure 4) to allow a small amount of flow (~0.002 psi/s) bypassing the dead-zone. Last, the open voltages for both valves are set to limit the flow (~0.2 psi/s) to set the maximum tuning speed.

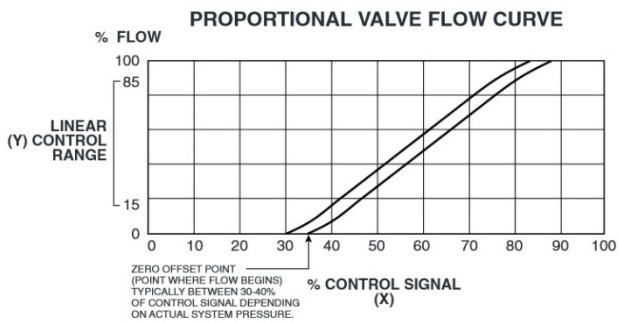

Figure 4: A typical proportional valve flow curve.

The valve calibration needs to be done at manifold pressure corresponding to the cavity operating frequency (322 MHz in our case). The tuner control logic based on the tuner error is shown in Fig. 5.

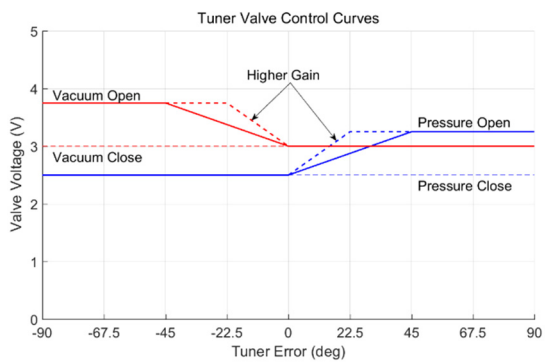

Figure 5: Pneumatic tuner control logic.

After solving different problems and making improvements, cavity phase and amplitude regulation was achieved at least 2-times better than the specification. Figure 6 shows the phase and amplitude error of a QWR at 110% of the designed field.

ISBN: 978-3-95450-184-7 doi:10.18429/JACoW-IPAC2018-WEXGBF3

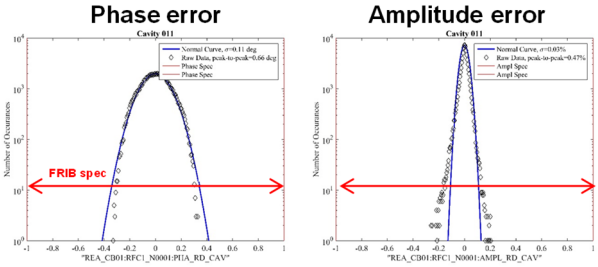

Figure 6: (LEFT) Phase error: 0.11 degrees RMS, 0.66 degrees peak-to-peak. (RIGHT) Amplitude error: 0.03% RMS, 0.47% peak-to-peak.

Solid-State Amplifiers

The architecture of the high power solid-state RF amplifiers is based on 2 kW amplifier drawers that can be combined for 4 kW and 8 kW. Each installed FRIB rack has four drawers, a power distribution unit, driver module, and controller unit. The amplifiers can be upgraded to six drawers in the case 12 kW is needed for linac upgrade or increased cavity bandwidth. Figure 7 shows the block diagram for a 2 x 4kW amplifier rack system.

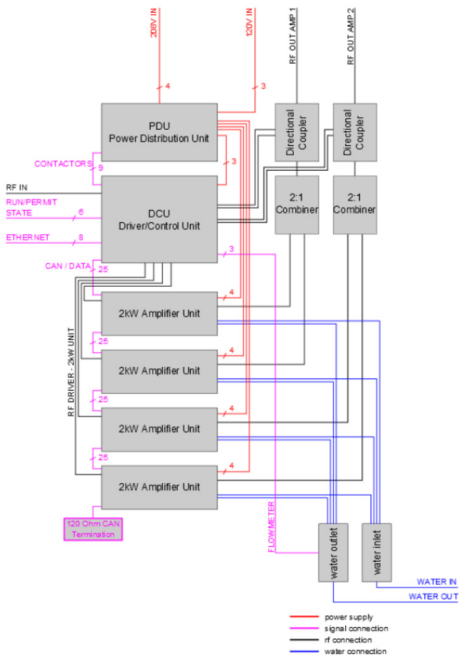

Figure 7: Block Diagram 2 x 4 kW RF amplifier.

The RF components (power splitters, pre-amplifiers, RF pallets, circulators, power combiners) vary by frequency, but most parts are common (power supplies, heat sinks, chassis, controller, etc.). All of the amplifiers use 1-5/8" SMS-style output connectors and transmission lines to keep the mechanical layout common for the 2-way and 4-way systems. Figure 8 is a photograph of the RF amplifier racks (2 x 4 kW).

Figure 8: (LEFT) RF amplifier racks in LS1. (RIGHT) Rear view of 2 x 4 kW amplifier rack (80.5 MHz).

The SRF cavities reflect up to 100% of forward power back to the amplifiers (depends on beam loading). The circulators, power combiners, directional couplers, and RF transmission lines must withstand voltage breakdown and insulator heating due to 2-times forward voltage and current (4-times power). A cavity discharge can also cause a surge of 4-times reflected power. The factory acceptance test (FAT) plans include pulsed and CW operation into a short circuit. Figure 9 shows the FAT setup.

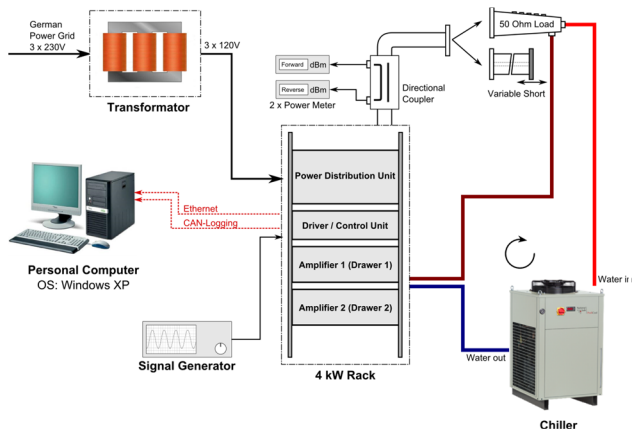

Figure 9: FAT Set Up for 2 x 4 kW RF amplifier.

A variable phase shifter simulates the reflections from the cavity with an arbitrary length transmission line (and/or cavity detuning). The FAT includes a 12 hour burn-in into the "worst case" phase (plus 8 hour burn-in at FRIB). All critical components are designed with 50% operating margin for high reliability. For example, the transistor cooling plate temperature does not exceed 60 degrees C in any case. Figure 10 shows test data during the phase shift test.

ISBN: 978-3-95450-184-7 doi:10.18429/JACoW-IPAC2018-WEXGBF3

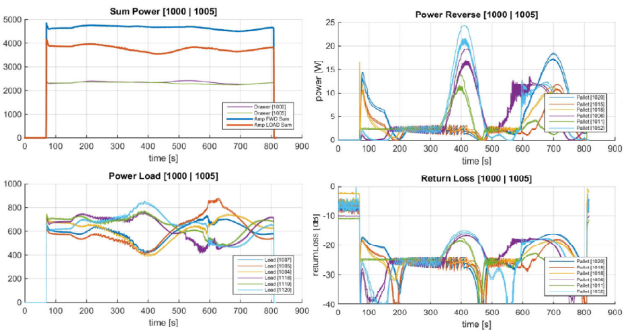

Figure 10: FAT data for phase shift into short circuit.

Early in the project it was realized that the narrow bandwidth and thermal sensitivity of the 80.5 MHz circulators was an issue for CW operation with 100% reflected power. In addition to using a 3-way topology to provide more margin per device, the amplifier supplier developed a circulator tracking method that minimizes return loss by varying the voltage on a coil wound around the ferrite core. The return loss was characterized for multiple devices by varying coil voltage and phase into the short circuit. The coefficients of the non-linear detuning equation were determined and stored in EEPROM [6]. The algorithm includes adaptation for changes in RF power and water temperature, including estimated detuning after RF is turned off.

Operation of the circulator tracking is reliable and has been tested during supplier FAT and FRIB acceptance testing with over 400 80.5 MHz amplifier drawers. The testing includes pulse, step-in, and CW operation. The software control itself is independent of frequency and power, but it is not needed for the 161 MHz and 322 MHz amplifiers. Figure 11 shows circulator characterization data and a simplified tracking algorithm.

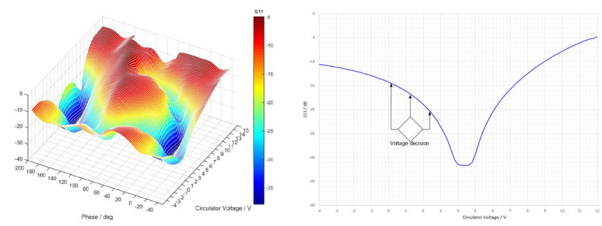

Figure 11: (LEFT) Circulator characterization data. (RIGHT) Simplified circulator tracking algorithm.

High Power Transmission Lines

The RF transmission lines connect the solid-state amplifiers in the rack room to the SRF cavities in the tunnel through concrete conduit banks. An insulated 20' wooden box mock-up was used for measuring temperatures in a single conduit. RF transmission lines with diameters 7/8" to 4-1/16" were placed inside the box and operated into a short circuit while scanning the inner and outer conductors. Next, thermal simulation were performed with ANSYS. The parameters for the single conduit model (insulated box) were adjusted to match the measured data, then a 2 by 8 conduit bank model was created that included the effects of convection and mutual heating from adjacent conduits. Based on the simulation data, the transmission lines for FRIB were selected in order to keep the inner conductor temperatures less than 80 degrees C inside the conduits (design goal) at the expected power levels for baseline operations and future 400 MeV upgrade.

RFQ COMMISSIONING

The FRIB RFQ amplifier is based on the NSCL ReA3 RFQ coaxial resonator tetrode amplifier with the following modifications: triode driver replaced by solid-state amplifier, upgraded to Allen Bradley PLC, and minor mechanical and electrical changes. The tube resonator and racks for power supplies, LLRF, controls and driver amplifier are shown in Figure 12.

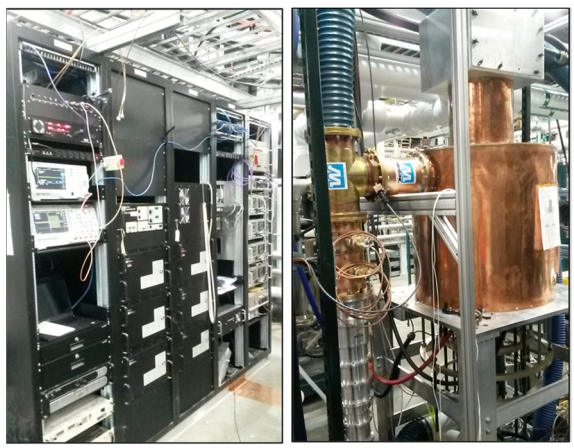

Figure 12: (LEFT) Power supplies, LLRF controller, driver amplifier. (RIGHT) RFQ tetrode tube amplifier.

The RFQ amplifier was load tested up to 100 kW with a LLRF controller in closed loop (CW and pulsed). However, when connected to the cavity the amplifier oscillated around 1 GHz. The tuning/load sliding shorts were adjusted to neutralize the amplifier. As a result, the overall gain was reduced and an improved input grid matching network was installed to minimize losses. To better protect the cavity, the LLRF controller interlock response time was reduced to <3 microseconds by moving the process to a faster clock domain.

Sparking during cavity commissioning caused frequent interlocks requiring a manual reset which slowed progress. During a spark, the low cavity impedance was transformed to a high load impedance at the amplifier output. This caused the amplifier output power to increase much faster than the LLRF controller could respond (the tube is a voltage-controlled current-source) resulting in overcurrent latched fault in the anode power supply. This issue was mitigated by inserting a ~quarter-wave extension in the RF transmission line. Now the forward power decreases slightly during a spark leading to a controlled turn off sequence (no latching). Figures 13 and 14 show the associated waveforms before and after the line extensions was installed.

ISBN: 978-3-95450-184-7 doi:10.18429/JACoW-IPAC2018-WEXGBF3

Figure 13: Before line extension. Forward power increases during spark event.

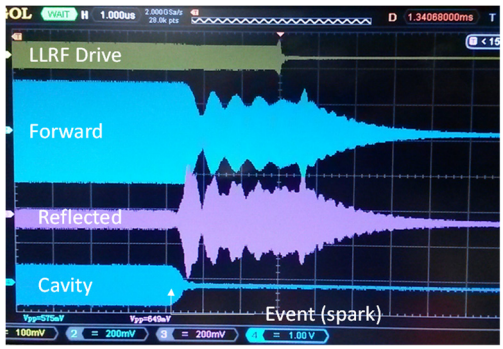

Figure 14: With line extension, forwarded power decreases during sparks (no latching faults).

Occasional delays occurred during cavity commission-ing due to overvoltage (OV) latches in the 15 kV anode power supply. The supplier (TDK) was consulted and the OV hardware limit in each 50 kW module was increased by replacing internal resistors. A glitch in the LLRF turn off waveform was also eliminated by updating the firm-ware to ramp down within 2 microseconds instead of using the RF switch in the output chain.

Finally, the LLRF firmware was updated (and cable added) to inhibit the synchronization pulses in the anode power supply to prevent charging of the output capacitors for >800 ns when the RF drive is turned off (Figure 15). These changes prevent unwanted latching to allow faster restarts after sparking events. The increased margin also allows the anode voltage to be increased (needed to reach 100 kW for uranium beam).

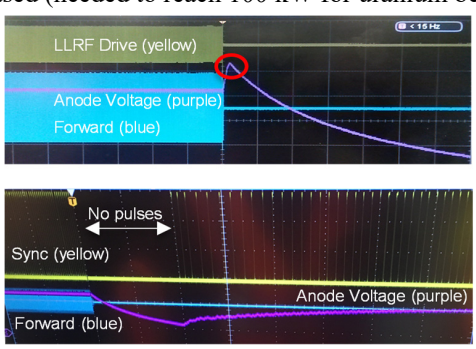

Figure 15: (TOP) Anode voltage increases after RF trips, causing frequent latched faults. (BOTTOM) Anode voltage is inhibited (no latching).

The RFQ was conditioned to 59 kW CW [7]. Typical RFQ power levels for Argon and Krypton beams are 38 kW and 49 kW, respectively (100 kW is needed for Uranium beam). The RFQ cavity will be conditioned to higher power, as needed. The amplitude and phase can be locked with the water skids in temperature and frequency control modes. To mitigate the x-ray hazard and permit personnel in the FRIB tunnel during FE operation, three of the six power supply modules have been locked out to limit the total available power. Table 3 shows the measured ampli-tude and phase for the FE RF systems.

Table 3: Summary of FE Amplitude and Phase Error

		MHB F1 (D0987)		MHB F2 (D0987)		MHB F3 (D0987)	
		Amplitude (Vp)	Phase (deg)	Amplitude (Vp)	Phase (deg)	Amplitude (Vp)	Phase (deg)
Set-point		5.2	45.0	9.2	20.0	4.4	10.0
Forward Power (W)		~ 70		~ 20		~ 20	
Peak Error (%, deg)	Meas.	0.294	0.240	0.473	0.336	0.518	0.358
	Spec.	< 1.5	< 1.5	< 1.5	< 1.5	< 1.5	< 1.5
RMS Error (%, deg)	Meas.	0.079	0.049	0.126	0.079	0.137	0.089
	Spec.	< 0.5	< 0.5	< 0.5	< 0.5	< 0.5	< 0.5

		RFQ (D1005)		MEBT (D1066)		MEBT (D1107)	
		Amplitude (Vp)	Phase (deg)	Amplitude (Vp)	Phase (deg)	Amplitude (Vp)	Phase (deg)
Set-point		12.88	20.0	3.56	10.0	6.00	15.0
Forward Power (W)		~ 40000		~ 1500		~ 1500	
Peak Error (%, deg)	Meas.	0.187	0.214	0.480	0.263	0.237	0.223
	Spec.	< 1.5	< 1.5	< 1.5	< 1.5	< 1.5	< 1.5
RMS Error (%, deg)	Meas.	0.025	0.048	0.060	0.055	0.037	0.054
	Spec.	< 0.5	< 0.5	< 0.5	< 0.5	< 0.5	< 0.5

SUMMARY

We have reported on the off-line testing and lessons learned for LLRF controllers and solid-state RF amplifiers. The challenges of commissioning the FRIB RFQ amplifier with cavity were presented. The FRIB front end has been commissioned with all RF devices running at or above KPP levels. The LLRF controllers and solid-state RF amplifiers have been installed in LS1 and preparations are on track for a readiness review in May 2018 and beam commissioning in July 2018 [8].

ACKNOWLEDGEMENTS

The authors would like to thank HBH Microwave, John Vincent (Ionetics; formerly at NSCL), John Lyles (LANL), Gary Zinkann (ANL), Sergey Sharamentov (ANL), Alexander Zaltsman (BNL), and Andy Tydeman (TDK Lambda) for their contributions to this work.

REFERENCES

[1] J. Wei et al., "The FRIB superconducting linac status and plans," LINAC'16, East Lansing, MI, USA, Sep. 2016, pp. 1-6.

[2] E. Pozdeyev et al., "FRIB front end construction and commissioning," IPAC'18, Vancouver, Canada, May 2018, paper MOZGBF1.

[3] S. Zhao et al., "Smooth switching design/implementation of the active disturbance rejection control," ASME 2017 International Design Engineering Technical Conferences, Cleveland, Ohio, pp. V009T07A012, 2017.

[4] J. Vincent et al., "On active disturbance rejection based control design for superconducting RF cavities," Nuclear Instru-ments and Methods in Physics Research A, vol. 643, no. 1, pp. 11-16, 2011.

ISBN: 978-3-95450-184-7 doi:10.18429/JACoW-IPAC2018-WEXGBF3

[5] S. Zhao et al., "Fixed-point implementation of active disturbance rejection control for superconducting radio frequency cavities," 2010 American Control Conference, Washington D.C., pp. 2693-2698, 2010.

[6] J. Klanjsek et al., "Circulator tracking - Software controlled circulators for 80.5 MHz power amplifier system", presented at CWRF2016, Grenoble, France.

[7] H. Ren et al., "Commissioning of the FRIB RFQ," IPAC'18, Vancouver, Canada, May 2018, paper TUPAL039.

[8] H. Ao et al., "Installation progress on FRIB beta=0.041 cyromodules toward beam commissioning," IPAC'18, Vancouver, Canada, May 2018, paper TUPAL037.